Density Functional Modeling of Long Range Magnetic Interactions in Binuclear Oxomolybdenum(V) Complexes

Alessandro Bencini,* Dante Gatteschi, and Federico Totti

Dipartimento di Chimica, Università di Firenze, Firenze, Italy

Delia Nieto Sanz

Departamento de Química Física Aplicada Universidad Autónoma de Madrid, Madrid, Spain

Jon A. Mc Cleverty and Michael D. Ward

School of Chemistry, University of Bristol, Bristol, U.K

Received: October 14, 1997; In Final Form: January 23, 1998

Magnetic exchange interactions have been calculated in the framework of the density functional (DF) theory for the quite rare exchange coupled binuclear compounds in which the magnetic centers belong to the 4d series: $[\{Mo^{V}(O)(Tp^*)Cl\}_2(\mu\text{-}X)]$, (where X is one of the dihydroxybenzene bridging ligands $[1,4\text{-}OC_6H_4O]^{2-}$ or $[1,3\text{-}OC_6H_4O]^{2-}$ and Tp* is tris(3,5-dimethylpyrazolyl)hydroborate. The exchange coupling constant *J* has been nicely reproduced with the use of the broken symmetry (BS) approach to avoid the multideterminant structure of the singlet state. Several local and gradient-corrected functionals have been tested. In order to determine relevant magneto-structural correlations between structural parameters and exchange coupling constants, we also performed calculations on model systems in which the relative orientations of the two molybdenum moieties with respect to the aromatic ring were varied. These calculations showed that the actual value of the magnetic coupling constant *J* is influenced not only by the topology, 1,3 or 1,4, of X, but a correlation with the relative orientation of the two branches containing the two Mo atoms exists. This magneto-structural correlation is bound to superexchange pathways, which are, therefore, also important in transmitting magnetic interactions through dihydroxybenzene ligands.

Introduction

The theoretical investigation of the magnetic interactions in polynuclear compounds has rapidly developed in the last few years thanks to the availability of efficient protocols for the calculation of the magnetic coupling between metal ions from first principles.[1] The understanding of the electronic origin of the magnetic interactions between metal centers, in fact, is of great importance in many fields, such as bio-[2] and solid-state inorganic chemistry,[3] and is a necessary prerequisite for developing efficient synthetic strategies for designing new magnetic materials.

The study of the properties of binuclear species is a good starting point for the understanding of more complex systems, such as molecular compounds with a three-dimensional magnetic structure. In fact, the HDVV spin Hamiltonian, the usual approach to the interpretation of the magnetic properties of large sized clusters, assumes that the interactions in large clusters can be calculated as a sum of two-center interactions.[4] Up until now detailed magneto-structural correlations have been established mainly for first-row transition metal complexes.[5] Second- and third-row systems have been much less investigated, although they are present in a number of biological[6] and inorganic systems.[7] Furthermore, much attention has been devoted to the exchange interactions mediated by rather small molecules, while long-range interactions have been generally less well studied theoretically.

Binuclear metal complexes in which the metals are bridged by an unsaturated ligand are of great interest for modeling electron transfer processes and magnetic exchange mechanisms.[8] Recently the complexes $[\{Mo^{V}(O)(Tp^*)Cl\}_2(\mu\text{-}X)]$, (where X is one of the dihydroxybenzene bridging ligands $[1,4\text{-}OC_6H_4O]^{2-}$ or $[1,3\text{-}OC_6H_4O]^{2-}$ and Tp* is tris(3,5-dimethylpyrazolyl)-hydroborate) were synthesized and structurally characterized. Despite the large size of the diamagnetic bridging ligand, X, both of the complexes (**1**,**4**) and (**1**,**3**) showed measurable magnetic exchange interactions between the paramagnetic metal (d^1, $S_i = {}^1/_2$) centers.[9]

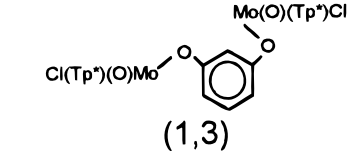

(1,3)

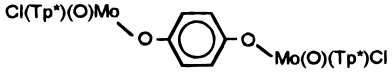

(1,4)

The magnetic behavior of each of the complexes (**1**,**4**) and (**1**,**3**) remarkably differs: complex (**1**,**4**) has a ground state corresponding to an $S = 0$ total spin state, arising from an antiferromagnetic coupling between the two $S_i = {}^1/_2$ spins of

10.1021/jp973328w CCC: $15.00
Published on Web 11/26/1998

the molybdenum atoms, while in (**1**,**3**) a triplet was found to be the ground state (ferromagnetic interaction). The observed triplet−singlet separations are 80 and −9.78 cm^{-1} for (**1**,**4**) and (**1**,**3**), respectively. The energy difference between the singlet and the triplet states is generally measured by fitting the temperature dependence of the magnetic susceptibility of the molecule to the energies of the eigenstates of the spin Hamiltonian

$$H = J\mathbf{S_1}\cdot\mathbf{S_2} \tag{1}$$

where $\mathbf{S_i}$ is the spin operator of center *i*.[4] In this formalism *J* is called the exchange coupling constant, and $J = E(S = 1) - E(S = 0)$.

ZINDO calculations[9] of the electronic structure of **1**,**3** and **1**,**4** which have shown that the magnetic orbitals are, in both cases, localized onto the metals and a spin-polarization mechanism, which correlates the unpaired electrons on the remote centers through polarization of the π bonding electrons, were proposed to account for their different magnetic behaviors. For the present compounds, in fact, the spin polarization of the bonding electrons leads to the pathway:

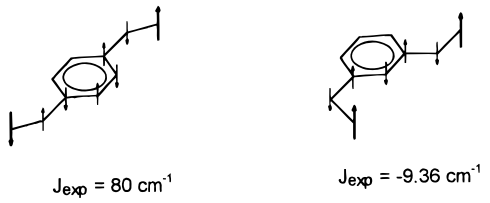

which follows the principle that electrons lying in overlapping atomic orbitals should be aligned antiparallel to each other.

In restricted Hartree−Fock theory (RHF), spin polarization is a direct consequence of the mixing of excited configurations, with the same symmetry, into the ground state (CI mixing). In unrestricted Hartree−Fock theory (UHF), which allows the orbitals to be different for different spins, spin polarization arises also from the different spatial distribution of the spin α and β caused by the fact that only electrons with the same spins have exchange integrals different from zero. The effect of the spin polarization is that the overall spin distribution can differ from what is expected from a charge delocalization mechanism, which is in turn bound to the symmetry of the molecule. For example, in the allyl radical, $CH_2CHCH_2^{\bullet}$, the unpaired electron is in a molecular orbital which has a node on the central carbon, while a negative spin density is experimentally found on that center.[10] Spin polarization is therefore always an effect which adds up to charge delocalization and is extremely difficult to compute, particularly in low-symmetry molecules, especially if more than one unpaired electron is present. Within the formalism of the active electron approximation,[4] charge delocalization is responsible for the interactions between the *magnetic orbitals*, orbitals containing the *magnetic electrons* (unpaired electrons close in energy) rather well localized onto single paramagnetic centers, leading to the onset of the exchange interactions. These are determined by two main factors: the exchange energy between electrons of equal spins which favors a parallel alignment of the spins between two adjacent centers (the so called *potential exchange* in the Anderson's theory) and the overlap between the magnetic orbitals, which gives rise to a transfer of the electron density between the paramagnetic centers and favors the antiparallel alignment of the spins (the so-called *kinetic exchange* in the Anderson theory). The interaction between magnetic orbitals can be direct (*direct exchange interaction*) or can occur via ligand centered orbitals (*superexchange interaction*). Qualitatively, the exchange interactions can be understood in term of exchange pathways, which connect the magnetic and ligand orbitals interacting by symmetry and can be regarded as the highways for the propagation of the correlation between the magnetic electrons.

Due to the complexity of the molecules at hand, HF theory cannot be applied with sufficient accuracy to compute their electronic structure, since an accurate description of the multiplet structure requires extensive post-Hartree-Fock corrections.[1d] We therefore applied the density functional (DF) formalism[11] to calculate the exchange coupling constant *J*, making use of the broken symmetry (BS) approach[12] to avoid the multideterminant structure of the singlet state. In order to determine relevant correlations between structural parameters and exchange coupling constants, we also performed calculations on model systems in which the relative orientations of the two molybdenum moieties with respect to the aromatic ring were varied.

To the best of our knowledge this is the first time that magneto-structural correlations based on ab initio calculations have been established for the quite rare exchange coupled binuclear compounds in which the magnetic centers belong to the 4d series.

Computational Details

The Amsterdam Density Functional (ADF) program package was used for all the calculations.[13] The standard bases provided with the program were used. Double-ζ STO bases were applied to the valence electrons of all atoms. The shells up to 4p for Mo and 1s for all the other non-hydrogen atoms were treated as frozen core. Different local (Xα, LDA[Stoll]) and nonlocal (BPW91c, B) functionals were used in order to estimate the dependence of the results on the actual forms of the functionals. The LDA[Stoll] approximation includes the local exchange−correlation potential of Vosko, Wilk, and Nusair[14] with added the Stoll's correlation[15] correction term. A value of $\alpha = 0.7$ was taken in the Xα functional. B and BPW91c both incorporate the gradient corrections to the exchange,[16] while BPW91c includes also the more recent gradient corrections to correlation of Perdew and Wang.[17] Quasi-relativistic effects have been also used. Overall calculations have been performed using the default values for single point runs: integration = 4.0 and scf-convergence = 1e−6. These criteria are generally used for computing magnetic observables.[1d]

The BS approach[12] was used for the calculation of the exchange coupling constant *J* of eq 1. In this formalism, the energy of the singlet state is computed by an approximate spin projection from the energy of a single determinant of broken spin and space symmetry built up by localizing spin up and spin down electrons onto the two molybdenum centers. Since the two Mo(V) ions are weakly interacting, the exchange coupling constant was computed using the expression:

$$J = 2(E(S = 1) - E(\mathrm{BS})) \tag{2}$$

which holds[18] when the overlap between the metal orbitals is much smaller than 1, which is likely to be the case here. In the opposite limit of strong overlap, the energy of the BS state approaches the energy of the singlet state and *J* in this case is given directly by the difference in energy between the triplet and the BS energies. Since the situations met in general are intermediate between these two limiting cases, use of eq 2 will lead to an overestimation of *J*.

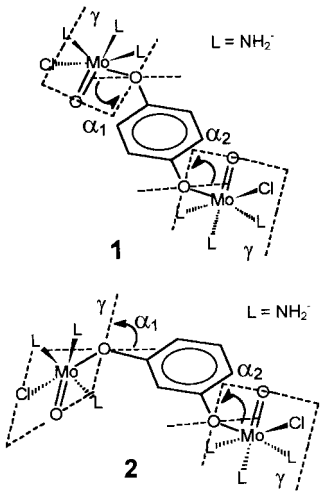

Figure 1. Schematic drawing of the molecular structures of the **1** and **2**. The α angles and γ the planes are also shown.

Results and Discussion

(**1**,**4**) has a crystallographic inversion center and the overall symmetry of the molecule is C_i, while in (**1**,**3**) no symmetry element is present (C_1 symmetry).[9] In order to limit the computational efforts, the Tp* ligand was modeled with three NH_2^- groups which simulate the π* interactions of the pyrazoles of the real ligand with Mo. These groups, in fact, possess a π orbital perpendicular to the NH_2 plane which mimics the interaction with the π orbital perpendicular to the pyrazoles of the Tp* ligands. The π orbitals of the NH_2^- groups were in fact oriented perpendicular to the pyrazole planes seen in the crystal structures of the real complexes. The model molecules we used had, therefore, the formula $\{[Mo(O)Cl(NH_2)_3]X-[Mo(O)Cl(NH_2)_3]\}^{4-}$. In (**1**,**4**) the Cl and O atoms are disordered[9] and, for the model (**1**,**4**), we have used for both metal centers the bond distances measured more accurately for the ordered metal centers of (**1**,**3**) (Mo−Cl = 2.340 Å, Mo═O = 1.747 Å).

The molybdenum atoms in both complexes are in a distorted octahedral coordination, MoO_2N_3Cl, where one of the oxygen atoms is doubly bonded to Mo to form the oxomolybdenum(V) cation as shown in Figure 1. Calling γ the MoO_2 plane and α the angle between the plane of the aromatic ring and the γ plane, the structures of the two molecules can be viewed as follows: in the (**1**,**4**) model, **1**, the two γ planes centered on the two Mo atoms are parallel to each other and α_1 and α_2 are fixed at the experimental values, −57.3° and 57.3°, respectively; in the (**1**,**3**) model, **2**, the dihedral angle between the γ planes is kept to the value of 100°, close to the experimental value, with $\alpha_1 = -38.4°$ and $\alpha_2 = 61.9°$.

The dependence of the computed *J* values on the actual form of the functionals used was also checked on the model systems **1** and **2**; all the other calculations were performed with the VWN(Stoll) functional. The effect of quasi-relativistic corrections[19] on the computed *J* values was also checked for the **1** and **2** cases.

The values of the exchange coupling constant *J*, computed on **1** and **2**, using different functionals, are reported in Table 1 and compared with the experimental findings. Both the sign and the magnitude of the exchange coupling constants agree well with the experimental findings. Local and nonlocal approximations to the exchange yield comparable results suggesting that the exchange part of the functional does not play a critical role. In other words, the computed *J* values do not significantly change when the form of the exchange functional varies from the Xα and the VWN expressions to the Becke one. The explicit form of the correlation term has, however, great importance: nonlocal corrections (BPW91c) gave the wrong sign of the exchange constant for the ferromagnetic complex **2**. The *J* values computed using the Xα and the LDA[Stoll] approaches better agree with the experimental data. This result is in line with the fact that the broken symmetry approach already includes part of the electronic correlation.[12] Stoll's correction removes the correlation between electrons with the same spin so that their contribution to the exchange−correlation energy is given only by the exchange part: this seems to properly account for the electron correlation giving the best agreement with the experimental findings. This situation has already been met in a number of different exchange coupled systems studied by DF methods.[1d] Quasi-relativistic corrections, too, correctly reproduce the sign, but they seem not to account the difference in absolute value of *J* for the two compounds.

TABLE 1: Effect of Different Functionals on the Computed *J* Values for Complexes 1 and 2

	$J(cm^{-1})$	
method of calculation	**1**	**2**
Xα	13	−6.06
VWN(Stoll)	41	−6.12
BPW91c[a]	17	−5.88
Becke−Stoll[a]	23	−4.74
(VWN)Stoll*(quasi-relative)	38	−36.00
exptl	80	−9.78(2)

[a] VWN formula has been used for the LDA part of the functional.

SCHEME 1

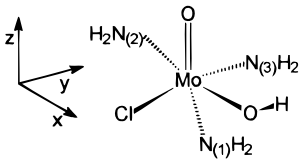

In the binuclear compounds **1** and **2**, the two SOMOs, obtained either from calculations on the triplet or on the broken symmetry state, are metal localized and quite well separated from the virtual orbitals. Since the singly occupied α and β orbitals coming from the BS calculation result largely localized onto the two different magnetic centers, they are generally considered as a nice description of the natural magnetic orbitals, and we will describe in more detail their composition. The magnetic orbitals computed for **1** and **2** differ significantly. Both in **1** and in **2** the magnetic orbitals are mainly 4d metal in character and localized on the two Mo(V) centers with large contributions from the atoms of the bridging ligand, but in **1** they also have a significant contribution of the 4d orbitals of the other metal center. The percent gross 4d atomic orbital populations (PGAOP4d) for the α and β magnetic orbitals of **1** and **2** are reported in Tables 2 and 3, respectively. The metal composition of the magnetic orbitals is a rather complicated mixture of 4d orbitals, due to the fact that the reference axes used are not properly oriented to reflect the idealized symmetry of the metal centers. In order to properly label the magnetic orbitals in the various geometrical arrangements of the systems, which are referred to different axes, we examined the electronic structure of the model mononuclear moiety shown in Scheme 1 below referred to a more meaningful reference system, where the Mo═O direction is taken as the *z* axis.

TABLE 2: Percent Gross Atomic Orbital Populations of the Magnetic Orbitals of 1[a] Obtained by BS Calculations

MO,[b] $\|\alpha\rangle$	ΔE, eV	ring	O_{1,p_y}	O_{1,p_z}	O_{2,p_y}	O_{2,p_z}	O_{3,p_x}	O_{3,p_y}	O_{3,p_z}	O_{4,p_x}	O_{4,p_y}	O_{4,p_z}
$\|$LUMO$\rangle$	0.59	2.5			1.6	1.9				2.4		
$\|$HOMO$\rangle$	0.00	2.0	2.0	1.9			3.7					

MO, $\|\alpha\rangle$	Mo_{1,z^2}	Mo_{1,x^2-y^2}	$Mo_{1,xy}$	$Mo_{1,xz}$	$Mo_{1,yz}$	Mo_{2,z^2}	Mo_{2,x^2-y^2}	$Mo_{2,xy}$	$Mo_{2,xz}$	$Mo_{2,yz}$	Cl_{1,p_x}	Cl_{1,p_y}	Cl_{1,p_x}	Cl_{2,p_x}	Cl_{2,p_z}
$\|$LUMO$\rangle$	0.2	0.4	0.8	0.2	0.1	28.5	19.7	7.3	7.0	6.1				4.1	1.1
$\|$HOMO$\rangle$	25.5	17.2	5.9	6.0	4.8	0.1	0.0	0.2	0.0	0.1	4.2	1.1			

MO, $\|\alpha\rangle$	$N_{1,1,p_y}$	$N_{1,1,p_z}$	$N_{1,2,p_y}$	$N_{1,2,p_z}$	$N_{1,3,p_y}$	$N_{2,1,p_y}$	$N_{2,1,p_z}$	$N_{1,1,p_y}$	$N_{2,2,p_z}$	$N_{2,3,p_y}$
$\|$LUMO$\rangle$			1.5			1.1	4.3			4.8
$\|$HOMO$\rangle$	2.5	9.1			6.8					

MO, $\|\beta\rangle$	ΔE, eV	ring	O_{1,p_y}	O_{1,p_z}	O_{2,p_z}	O_{2,p_z}	O_{3,p_x}	O_{3,p_y}	O_{3,p_z}	O_{4,p_x}	O_{4,p_y}	O_{4,p_z}
$\|$LUMO$\rangle$	0.59	2.5	1.6	1.9			2.4					
$\|$HOMO$\rangle$	0.00	2.0			2.0	1.9				3.8		

MO, $\|\beta\rangle$	Mo_{1,z^2}	Mo_{1,x^2-y^2}	$Mo_{1,xy}$	$Mo_{1,xz}$	$Mo_{1,yz}$	Mo_{2,z^2}	Mo_{2,x^2-y^2}	$Mo_{2,xy}$	$Mo_{2,xz}$	$Mo_{2,yz}$	Cl_{1,p_x}	Cl_{1,p_z}	Cl_{2,p_x}	Cl_{2,p_z}
$\|$LUMO$\rangle$	28.5	19.7	7.3	7.0	6.1	0.2	0.4	0.3	0.2	0.1	4.2			
$\|$HOMO$\rangle$	0.1	0.0	0.2	0.0	0.1	25.5	17.2	5.9	6.1	4.8			4.2	1.1

MO, $\|\beta\rangle$	$N_{1,1,p_y}$	$N_{1,1,p_z}$	$N_{1,2,p_y}$	$N_{1,2,p_z}$	$N_{1,3,p_y}$	$N_{2,1,p_y}$	$N_{2,1,p_z}$	$N_{1,1,p_y}$	$N_{2,2,p_z}$	$N_{2,3,p_y}$
$\|$LUMO$\rangle$	1.1	4.3			4.8					
$\|$HOMO$\rangle$						2.5	9.1			6.8

[a] Ring contains the total carbon p_y orbital populations. [b] Orbital populations <1% are shown only for Mo atoms.

TABLE 3: Percent Gross Atomic Orbital Populations of the Magnetic Orbitals of 2[a] Obtained by BS Calculations

MO,[b] $\|\alpha\rangle$	ring	O_{1,p_x}	O_{1,p_z}	O_{2,p_z}	O_{4,p_y}	$Cl_{1,1,p_z}$	$Cl_{1,1,p_y}$
$\|$LUMO$\rangle$	9.5			2.2	1.2		
$\|$HOMO$\rangle$	2.2	2.1	1.2			1.3	3.8

Mo,[b] $\|\alpha\rangle$	Mo_{1,z^2}	Mo_{1,x^2-y^2}	$Mo_{1,xy}$	$Mo_{1,xz}$	$Mo_{1,yz}$	Mo_{2,x^2-y^2}	$Mo_{2,xy}$	$Mo_{2,xz}$	$Mo_{2,yz}$	$N_{1,2,p_y}$	$N_{1,2,p_z}$	$N_{1,3,p_z}$	$N_{2,3,p_z}$
$\|$LUMO$\rangle$	0.0	0.0	0.0	0.0	0.0	21.9	15.0	26.5	4.5				9.8
$\|$HOMO$\rangle$	2.6	6.4	33.7	0.5	9.2	0.0	0.0	0.0	0.0	3.4	2.7	18.2	

MO,[b] $\|\beta\rangle$	ring	O_{1,p_x}	O_{2,p_z}	O_{3,p_x}	O_{4,p_x}
$\|$LUMO$\rangle$	4.6	2.1		1.2	
$\|$HOMO$\rangle$	4.8		3.1		2.0

MO,[b] $\|\beta\rangle$	Mo_{1,z^2}	Mo_{1,x^2-y^2}	$Mo_{1,xy}$	$Mo_{1,yz}$	Mo_{2,x^2-y^2}	$Mo_{2,xy}$	$Mo_{2,xz}$	$Mo_{2,yz}$	$Cl_{1,1,p_y}$	$Cl_{2,1,p_x}$	$Cl_{2,1,p_y}$
$\|$LUMO$\rangle$	1.1	5.8	46.4	12.4	0.0	0.0	0.0	0.0	4.8		
$\|$HOMO$\rangle$	0.0	0.0	0.0	0.0	21.3	14.0	22.0	3.7		3.8	1.6

MO,[b] $\|\beta\rangle$	$N_{1,1,p_y}$	$N_{1,2,p_y}$	$N_{1,3,p_z}$	$N_{2,1,p_y}$	$N_{2,1,p_z}$	$N_{2,2,p_z}$	$N_{2,3,p_z}$
$\|$LUMO$\rangle$	1.5	1.1	9.3				
$\|$HOMO$\rangle$		1.8		1.0	1.6	1.0	12.4

[a] Ring contains the total carbon p_y orbital populations. [b] Orbital populations >1% are shown only for the Mo atoms.

The energies and composition of the highest occupied and lowest unoccupied orbitals are reported in Table 4. Because of the short molybdenum−oxygen distance (1.8 Å) the d_{z^2}, d_{xz}, and d_{yz} orbitals are largely destabilized by the antibonding interactions with the p_z, p_x, and p_y orbitals of the O atom (σ and π interactions respectively for p_z and (p_x, p_y)). Among the other d orbitals, the $d_{x^2-y^2}$ one is destabilized more than the d_{xy} by σ interactions with the equatorial ligands and lies at the highest energy. The SOMO is therefore mainly composed by the d_{xy} orbital, which is destabilized by the π^* interaction with the p_y orbital of Cl. The complex linear combinations of 4d orbitals, shown in Table 2, represent the mainly $4d_{xy}$ metal orbitals of the two molybdenum centers referred to in our different axis system. The composition of the magnetic orbitals show that a superexchange mechanism is important in transferring the unpaired electron density from one center to the other: in **2** the superexchange pathway occurs only via the π system of the bridging ligand, while in **1** also a direct delocalization onto the other metal center is found. In **1** this delocalization mechanism involves large contribution between nonorthogonal orbitals (essentially $4d_{xy}$) and can possibly lead to an antiferromagnetic contribution to the overall exchange interaction.

In the literature, the calculation of the distribution of spin density in paramagnetic molecules is becoming important since it is often used to interpret polarized neutron diffraction data, which are employed to deduce experimental evidence for exchange pathways and mechanisms.[20] The term spin densities is generally used in a loose sense to indicate gross atomic Mulliken spin populations,[21] and their use for the fitting of polarized neutron diffraction data has also received some criticism.[22] In particular, when the molecule has more than one unpaired electron, a good description of the low-spin states can be obtained only using a multiconfiguration wave function which may require large computational efforts. DF methods cannot give, therefore, a good description of the low-spin states. However, the broken symmetry state, whose energy is a weighted average of the energies of the various spin multiplets arising from the exchange interaction, is often used for the

TABLE 4: Percent Gross Atomic Orbital Populations for the α and *β* Magnetic Orbitals of the Mononuclear Moiety

MO, $\|\alpha\rangle$	ΔE, eV	Mo_{z^2}	$Mo_{x^2-y^2}$	Mo_{xy}	Mo_{xz}	Mo_{yz}	Cl_{1,p_x}	Cl_{1,p_z}	O_{1,p_y}	O_{2,p_y}	O_{2,p_z}
|LUMO+2⟩	1.20	2.2				32.5		1.2			
|LUMO+1⟩	1.03		2.2			20.9		1.2			
|LUMO⟩	0.59		2.5		56.3				21.2		5.1
|SOMO⟩	0.00			57.4			4.6		1.1	6.1	

MO, $\|\alpha\rangle$	N_{1,p_y}	N_{1,p_z}	N_{2,p_x}	N_{2,p_y}	N_{2,p_z}	N_{3,p_y}	N_{3,p_z}
|LUMO+2⟩				3.8			
|LUMO+1⟩	2.0	2.6				2.2	
|LUMO⟩					1.3		
|SOMO⟩			4.1	2.4	8.9		5.8

MO, $\|\beta\rangle$	ΔE, eV	Mo_{z^2}	$Mo_{x^2-y^2}$	Mo_{xy}	Mo_{xz}	Mo_{yz}	Cl_{1,p_x}	Cl_{1,p_z}	O_{1,p_x}	O_{2,p_y}	O_{2,p_z}
|LUMO+3⟩	1.21	2.7				36.0		1.5		20.4	1.5
|LUMO+2⟩	0.75		1.2	2.2					1.0		
|LUMO+1⟩	0.56		2.6		58.3				18.1		4.9
|LUMO⟩	0.00			68.0			4.6			5.5	

MO, $\|\beta\rangle$	N_{1,p_z}	N_{2,p_x}	N_{2,p_y}	N_{2,p_z}	N_{3,p_y}	N_{3,p_z}
|LUMO+3⟩	5.0	2.0				1.7
|LUMO+2⟩					2.2	
|LUMO+1⟩				1.5		
|LUMO⟩		2.1	4.8			

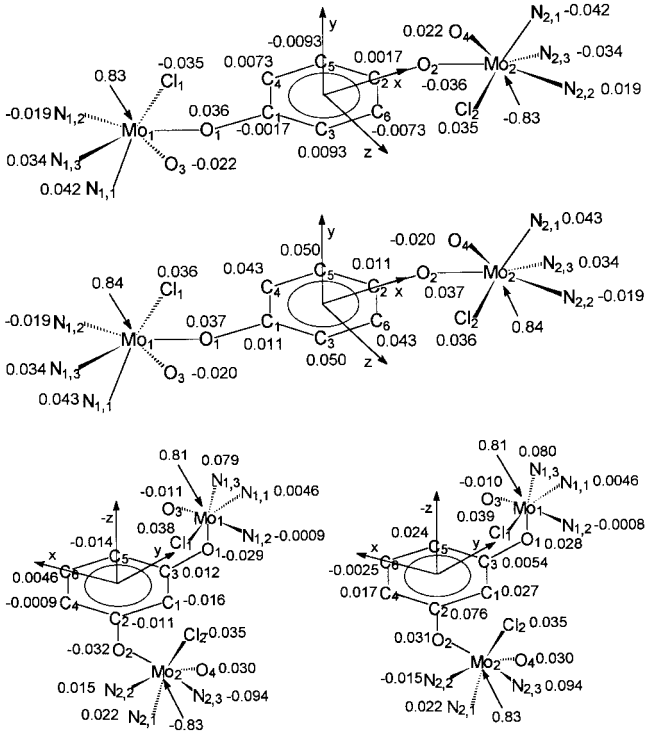

Figure 2. (a) Gross atomic spin populations computed for **1** for the broken symmetry (top) and triplet state (bottom). (b) Gross atomic spin populations computed for **2** for the broken symmetry (left) and triplet state (right).

description of the low-spin states.[23] Due to the relevance that spin densities can have, we report in Figure 2a,b the gross atomic spin populations of **1** and **2**, respectively, computed on the $S = 1$ and the BS state. The BS states of **1** and **2** show alternating spin densities with a distribution of values and signs, which obeys the total symmetry of the complexes and the localization of the α and *β* electrons onto the different metal centers. This alternation of spins is lost in the triplet state. In **1** and **2** a significant amount of spin density is computed on the aromatic bridging ligand both for the broken symmetry and triplet states. In **2** the largest spin density on the aromatic ring is computed on the carbons which form the shorter aromatic spin pathway.

TABLE 5: *J* Values (cm^{-1}) Calculated for $M_{1,2}$(1,3) and $M_{1,2}$(1,4) for Different α_1, α_2 Values

models	$\alpha_1 = \alpha_2 = 0°$	$\alpha_1 = \alpha_2 = 45°$	$\alpha_1 = 0°$, $\alpha_2 = 45°$	$\alpha_1 = \alpha_2 = 90°$	$\alpha_1 = 0°$, $\alpha_2 = 90°$
$M_{1,2}$(1,4)	1335	163	618	1	−68
$M_{1,2}$(1,3)	80	27	−11	−4	16

From the calculations of the singlet−triplet separation on **1** and **2**, it appears that superexchange mechanisms can have important effects in the propagation of the magnetic interaction between the two metal centers. In this case the relative intramolecular orientations of the two $[(NH_2)OMo(O-R)Cl]^{2-}$ fragments, and in particular of the *γ* planes, can modulate, together with the spin polarization effects, both the magnitude and the sign of the exchange coupling constant *J*. In order to establish magneto-structural correlations, we performed calculations by varying the α_i angles in both the (**1**,**4**) and (**1**,**3**) model complexes. Two kinds of variation were performed: in the first one, we kept the two *γ* planes parallel to each other; in the second one we varied the angle between them, while keeping $\alpha_1 = 0°$. We label these model systems as $\mathbf{M_1}$ and $\mathbf{M_2}$, respectively. We will have, therefore, $\mathbf{M_1}$**(1,3)**, $\mathbf{M_2}$**(1,3)**, $\mathbf{M_1}$**(1,4)**, and $\mathbf{M_2}$**(1,4)** as model systems. In $\mathbf{M_1}$**(1,4)** the overall symmetry of the molecule is C_i, while C_1 was applied to all the other cases. Using the LDA[Stoll] functionals, we have computed the effect of the values of the α_1 and α_2 angles on *J* for the model systems $\mathbf{M_1}$ and $\mathbf{M_2}$. The results of the calculations are shown in Table 5. The computed *J* values dramatically depend on the geometrical arrangement. In particular both ferro- and antiferromagnetic interactions can be obtained irrespective of the topology (1,3- or 1,4-) of the metals: it is the relative orientation of the *γ* planes which appears to determine the sign and magnitude of the interaction. For the geometries $\alpha_1 = 0°$ and $\alpha_2 = 90°$ for complex 1,4- and $\alpha_1 = \alpha_2 = 0°$ for complex 1,3-, we have computed a ground state which has not yet experimentally observed: the **1**,**4** complex has a ferromagnetic behavior ($J = -68$ cm^{-1}) while the **1**,**3** complex has an antiferromagnetic one ($J = 80$ cm^{-1}). The magnetic behavior can therefore be explained assuming that a superexchange mechanism is dominant: this can be better understood with the aid of Figures 3[24] and 4[24], where the isodensity surfaces of the magnetic orbitals of $\mathbf{M_{1,2}}$**(1,4)** and

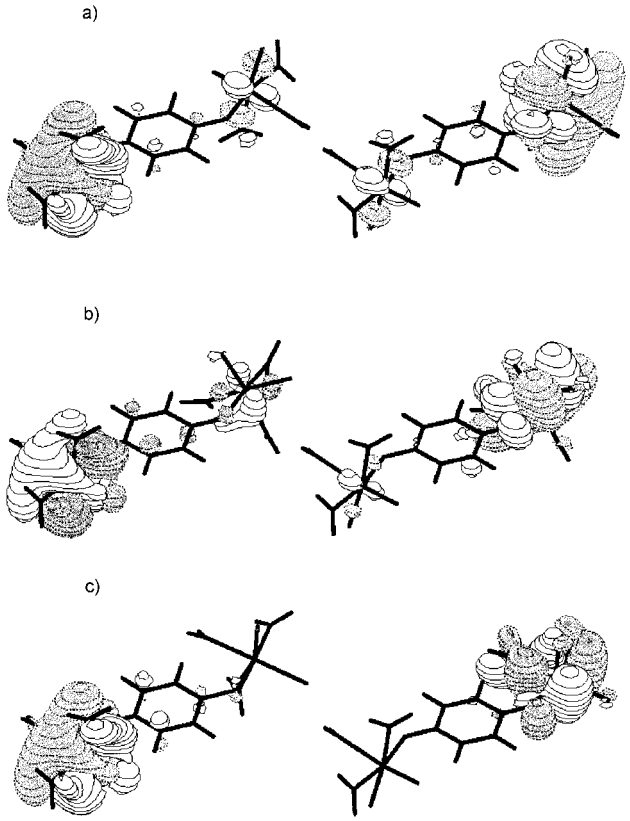

Figure 3. Isodensity surfaces ($\psi = 0.05$ (e/b^3)$^{1/2}$) of the magnetic orbitals of the $\mathbf{M_{1,2}(1,4)}$ models for the cases (a) $\alpha_1 = \alpha_2 = 0°$, (b) $\alpha_1 = 0°$ and $\alpha_2 = 45°$, and (c) $\alpha_1 = 0°$ and $\alpha_2 = 90°$.

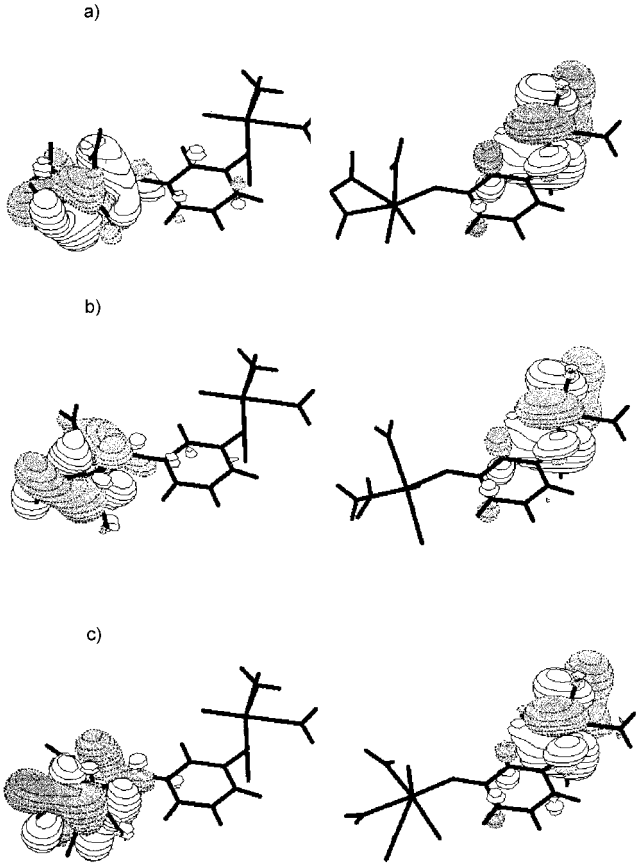

Figure 4. Isodensity surfaces ($\psi = 0.05$ (e/b^3)$^{1/2}$) of the magnetic orbitals of the $\mathbf{M_{1,2}(1,3)}$ models for the cases (a) $\alpha_1 = \alpha_2 = 0°$, (b) $\alpha_1 = 0°$ and $\alpha_2 = 45°$, and (c) $\alpha_1 = 0°$ and $\alpha_2 = 90°$.

$\mathbf{M_{1,2}(1.3)}$ calculated for different α values are reported. For the $\mathbf{M_1}$ case (Figure 2), a decrease of delocalization of the magnetic orbitals onto both the magnetic centers passing from the (a) $\alpha_1 = \alpha_2 = 0°$ to (c) $\alpha_1 = 0°$ and $\alpha_2 = 90°$ geometric arrangements is apparent. The magnetic orbitals pass from a strong overlapping case (a) to one (c) in which they are orthogonal with no possibility to interact through the bridging ligand. For the $\mathbf{M_2}$ complexes, the same trend has been computed, but in this case the delocalization is limited to the aromatic ring.

The difference in the absolute values of *J*, obtained for the different geometric arrangements, can be qualitatively understood if one considers that the intrinsic nature of the coordination **1**,**4**- vs **1**,**3**- allows, respectively, a large or small delocalization of the magnetic orbitals onto the bridging ligand and the magnetic centers. Considering that the spin-polarization contributions are due, in first approximation, to the magnetic orbitals, we propose a qualitative scheme based on the overlap between the magnetic orbitals to describe how the spins can polarize each other from one magnetic center to another. An antiparallel alignment of the arrows will be achieved when the overlap between the magnetic orbitals differs from zero, while a parallel alignment will arise when the overlap is nearly zero (orthogonal magnetic orbitals). These intuitive concepts, which surely require a more precise operational definition to be developed, are widely used among magneto-chemists to associate concepts to the numbers obtained from quantitative calculations of the exchange coupling constants or even to qualitatively rationalize magnetic exchange interactions.[4,9]

The concepts of superexchange and spin-polarization pathways can be used to qualitatively interpret the variation of the magnitude of the computed *J* values. The two mechanisms are pictorially compared in Figure 5 for the cases $\alpha_1 = \alpha_2 = 0°$, $\alpha_1 = \alpha_2 = 90°$, and $\alpha_1 = 0°$ and $\alpha_2 = 90°$. Applying the concepts outlined above, when the topology of the fragments is such that the $4d_{xy}$ orbital of Mo cannot efficiently overlap with the p_y orbital of the equatorial oxygen, we have assigned a parallel distribution of the spin density from the molybdenum onto the adjacent atom. This spin distribution was also observed in the BS calculations, as shown in Figure 2a,b for the experimental geometries **1** and **2**. Figure 5 shows that the largest $|J|$ values correspond to the situations in which the two

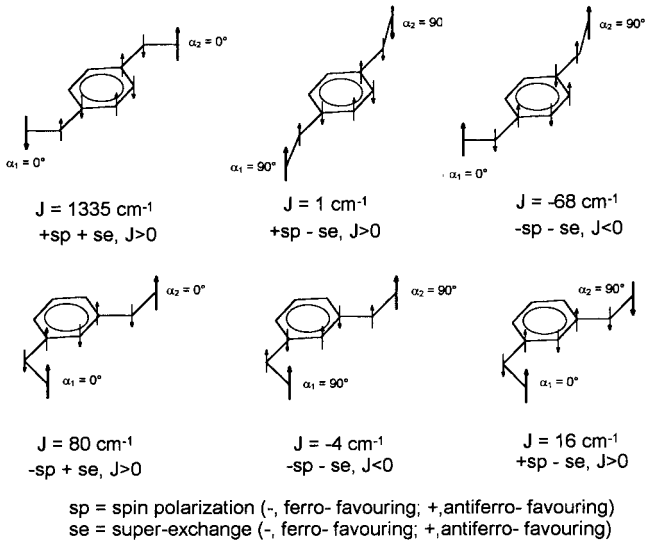

Figure 5. Comparison of the superexchange and the spin-polarization mechanisms in determining the absolute values of *J* for different α values.

mechanisms, superexchange and spin polarization, have the same effects either ferro- or antiferromagnetic. Unfortunately, at the present level of approximation, we cannot separate the effects of the two mechanisms at the computational level. This will be the goal to be achieved for the complete understanding of the physical mechanism of spin coupling in transition metal compounds.

Conclusions

Density functional calculations have nicely reproduced the experimental singlet−triplet splitting observed in [{Mo^{V}(O)(Tp*)Cl}$_2$(μ-X)] (where X is one of the dihydroxybenzene bridging ligands [1,4-OC_6H_4O]$^{2-}$ or [1,3-OC_6H_4O]$^{2-}$ and Tp* is tris(3,5-dimethylpyrazolyl)hydroborate), two unusual complexes in which the paramagnetic centers are separated by a large diamagnetic ligand. These calculations have shown that the actual value of the magnetic coupling constant *J* is influenced not only by the topology, **1**,**3** or **1**,**4**, of X, but a correlation with the angle α defined in Figure 1 exists. This magneto-structural correlation is bound to superexchange pathways, which are therefore important in transmitting magnetic interactions also through dihydroxybenzene ligands, in addition to spin polarization effects.

The present results encourage us to extend the characterization of the magnetic exchange pathways to other molybdenum complexes: binuclear and trinuclear compounds are currently under investigation.

References and Notes

(1) (a) De Loth, P.; Cassoux, P.; Daudey, J. P.; Malrieu, J. P. *J. Am. Chem. Soc.* **1981**, *103*, 4007. (b) Castell, O; Miralles, J.; Caballol, R. *Chem. Phys.* **1994**, *179*, 377. (c) Wang C.; Fink K., Staemmler V. *Chem. Phys.* **1981**, *74*, 5737. (d) Bencini, A.; Totti, F; Daul, C.; Doclo, K; Fantucci, P; Barone, V. *Inorg. Chem.* **1997**, *36*, 5022.

(2) Holm, R. H., Solomon, E. I., Eds. *Bioinorganic Enzymology; Coord. Chem. Rev.* **1996**, *96*, 2237−3042.

(3) Khan, O.; Pei, Y.; Journaux, Y. In *Inorganic Materials*; Bruce, D. W., O'Hare, D., Eds.; Wiley: Chichester, England.

(4) Kahn, O. *Molecular Magnetism*; VCH: New York, 1993.

(5) (a) Hodgson, D. J. *Inorg. Chem.* **1976**, *15*, 3174. (b) Hodgson, D. J. *Prog. Inorg. Chem.* **1976**, *18*, 796. (c) Charlot, M. F.; Khan, O.; Jeannin, S.; Jeannin, Y. *Inorg. Chem.* **1980**, *19*, 1410. (d) Melník, M. *Coord. Chem. Rev.* **1982**, *42*, 259. (e) Bencini, A. *J. Chem. Phys.* **1989**, *86*, 763.

(6) (a) Koppenhagen, V. B.; Elsenhans, B.; Wagner, F.; Pfiffener, J. J. *J. Biol. Chem.* **1974**, *249*, 6532. (b) Koppenhagen, V. B.; Elsenhans, B., Wagner, F.; Pfiffener, J. J. In *Electron Transfer in Inorganic, Organic, and Biological Systems*; Bolton, J. R., Mataga, N., McLendon, G., Eds. Advances in Chemistry 228; American Chemical Society: Washington, DC, 1991; Chapter 12.

(7) Johnson, M. K., King, R. B., Kurtz, D. M., Jr., Kutal, C., Norton, M. L., Scott, R. A., Eds. *Electron Transfer in Biology and the Solid State: Inorganic Compounds with Unusual Properties*; Advances in Chemistry 226; American Chemical Society: Washington, DC, 1990; Chapter 19.

(8) Ung, V. A.; Cargill Thompson, A. M. W.; Bardwell, D. A.; Gatteschi, D.; Jeffrey, J. C.; McCleverty, J. A.; Totti, F.; Ward, M. D. *Inorg. Chem.* **1997**, *36*, 3447.

(9) Ung, V. A.; Bardwell, D. A.; Jeffery, J. C.; Maher, J. P.; McCleverty, J. A.; Ward, M. D.; Williamson, A. *Inorg. Chem.* **1996**, 35, 5290.

(10) Wertz, J. E.; Bolton, J. R. *Electron Spin Resonance; Elementary Theory and Practical Applications*; McGraw Hill: New York, 1972.

(11) Parr, R. G.; Yang, W. *Density-Functional Theory of Atoms and Molecules*; Oxford University Press: New York, 1989.

(12) Noodleman, L. *J. Chem. Phys.* **1981**, *74*, 5737.

(13) Velde, G. te. *ADF 2.0.1. Theoretical Chemistry; Vrije Universiteit*.

(14) Vosko, S. H.; Wilk, L.; Nusair, M. *Can. J. Phys.* **1980**, *58*, 1200.

(15) Stoll, H.; Pavlidou, C. M. E.; Preuss, H. *Theoret. Chim. Acta* **1978**, *49*, 143.

(16) Becke, A. D. *Phys. Rev. A* **1988**, *38*, 3098.

(17) Perdew, J. P.; Wang, Y. *Phys. Rev. B* **1992**, *45*, 13244.

(18) Noodleman, L.; Norman, J. G., Jr. *J. Chem. Phys.* **1979**, *70*, 4093.

(19) Boerrigter, P. M. *Spectroscopy and Bonding of Heavy Element Compounds*, Ph.D. Thesis, Department of Chemistry, Vrije Universiteit, Amsterdam).

(20) McConnell, *J. Chem. Phys.* **1963**, *39*, 1910.

(21) Mulliken, R. S. *J. Chem. Phys.* **1955**, *23*, 1833.

(22) (a) Gillon, B.; Schweizer, J. In *Molecules in Physics, Chemistry and Biology*; Maruani, J., Ed.; Kluwer Academic: Dordrecht, 1989; Vol. 2, p 111. (b) Papoular, R. J.; Ressouche, E.; Schweizer, J.; Zheludev, A. In *Maximum Entropy and Bayesian Methods*; Mohamad-Jafari, A., Demoment, G., Eds.; Kluwer Academic: Dordrecht, 1993; Vol. 53, p 311. (c) Zheludev, A.; Barone, V.; Bonnet, M.; Delley, B.; Grand, A.; Ressouche, E.; Rey, P.; Subra, R.; Schweizer, J. *J. Am. Chem. Soc.* **1994**, *116*, 2019.

(23) (a) Lovell, T.; McGrady, J. E.; Stranger, R.; Macgregor, S. A. *Inorg. Chem.* **1996**, *35*, 3079. (b) Edgecombe, K. E.; Becke, A. D. *Chem. Phys. Lett.* **1995**, *244*, 427.

(24) These plots have been obtained using the program MOLDEN, by G. Schaftenaar, properly modified to elaborate the ADF results by F. Mariotti, Dipartimento di Chimica, Univeristà di Firenze.